REVIEWS

Journal of Semiconductors
(2021) 42, 071901
doi: 10.1088/1674-4926/42/7/071901

Suppressed light-induced phase transition of $CsPbBr_2I$: Strategies, progress and applications in the photovoltaic field

Hushan Zhang and Zhiwen Jin†

School of Physical Science and Technology & Key Laboratory of Special Function Materials and Structure Design (MoE) & National & Local Joint Engineering Laboratory for Optical Conversion Materials and Technology, Lanzhou University, Lanzhou 730000, China

Abstract: The rapid rise in the power conversion efficiency (PCE) of $CsPbBr_2I$-based perovskite solar cells (PSCs), from 4.7% in 2016 to 11.08% in 2020, render it a promising material for use in photovoltaic devices. However, the phase stability and current hysteresis caused by photo-induced phase segregation in $CsPbBr_2I$ represent major obstacles to further improvements in the PCE for such devices. In this review, we describe the basic structure and optical properties of $CsPbBr_2I$, and systematically elaborate on the mechanism of the phase transition. We then discuss the strategies in progress to suppress phase transition in $CsPbBr_2I$, and their potential application in the photovoltaic field. Finally, challenges and application prospects for $CsPbBr_2I$ PSCs are summarized in the final section of this article.

Key words: perovskite; $CsPbBr_2I$; stability; phase transition; phase segregation

Citation: H S Zhang and Z W Jin, Suppressed light-induced phase transition of $CsPbBr_2I$: Strategies, progress and applications in the photovoltaic field[J]. *J. Semicond.*, 2021, 42(7), 071901. http://doi.org/10.1088/1674-4926/42/7/071901

1. Introduction

The energy crisis caused by the massive consumption of fossil fuels is a serious problem that must be addressed today. Since the Second World War, many countries have committed to the development of renewable energy, including nuclear energy, wind energy, solar energy and tidal energy; of these, solar energy is favored, being both eco-friendly and economical. In the last decade, significant progress has been made in the field of perovskite solar cells (PSCs), with third-generation photovoltaic materials representing a promising candidate to replace monocrystalline silicon. Given perovskite's power conversion efficiency (PCE), ranging from 5.8% to 25.5%[1–5], organic–inorganic halide PSCs have become the backbone of perovskite efficiency growth, due to their wide light absorption, excellent carrier mobility, and electron diffusion length. However, volatile cations, such as methylammonium (MA^+) and formamidine (FA^+), used in organic–inorganic halide solar cells are not stable under light, heat and temperature, making them particularly vulnerable to degradation due to environmental conditions, and as such, unmarketable[6, 7]. These cations degrade readily, and are therefore not suitable for commercial use[8]. In response to this, researchers have attempted to introduce inorganic cesium (Cs^+) in place of organic cations, to form all-inorganic perovskites[9–12].

Of the various all-inorganic perovskites, $CsPbI_3$ and $CsPbI_2Br$ have relatively narrow bandgaps, (E_g), together with a wide light absorption range, and have achieved efficiencies of about 19%[13–15]. However, when the external temperature changes, both are prone to thermodynamic phase transition into a non-perovskite phase, resulting in extremely low efficiency, which also restricts their development for commercial use. In contrast, $CsPbBr_3$ shows excellent thermal stability under environmental stress[16–18]. Unfortunately, the large band gap (2.3 eV) of $CsPbBr_3$ limits the absorption of light, restricting its further development. Taking into account the issues above, it is widely understood that $CsPbBr_2I$ has a more suitable band gap (2.08 eV) as compared with $CsPbBr_3$ (2.3 eV), and demonstrates excellent thermal stability, as compared with $CsPbI_3$ or $CsPbI_2Br$. Since $CsPbBr_2I$ forms a high-temperature phase at high temperature, and enters a tetragonal phase when cooled to room temperature, it exhibits relatively superior thermal stability, meaning that $CsPbBr_2I$ does not undergo thermodynamic phase transition when the external temperature changes[19–21].

$CsPbBr_2I$ was first discussed by Ma *et al.* in 2016[22, 23]. With process optimization and ion doping, its PCE attained a maximum of 11.08%. However, the PCE of $CsPbBr_2I$ still lags far behind other types of perovskite (e.g., $CsPbI_3$ or $CsPbI_2Br$). The main reason for this is the serious phase segregation inside the $CsPbBr_2I$. Under illumination, halide ions migrate to the grain boundary or crystal surface, so that the concentration of halide ions in the grain boundary or crystal surface is too high, which seriously affects ions migration, and leads to ions enrichment, thereby causing phase segregation. Phase segregation changes the absorption range of visible light by changing the band gap of the $CsPbBr_2I$, resulting in lower efficiency. As such, the actual PCE of $CsPbBr_2I$ was far lower than the theoretical efficiency.

Phase segregation has always been the most worthwhile area of study in relation to hybrid halide PSCs. For example, I^- and Br^- in the crystal lattice of $MAPb(Br_xI_{1-x})_3$ and $CsPb(I_{1-x}Br_x)_3$ migrate due to the halide ions obtaining sufficient migration energy under light[24, 25]. Due to the high energy of the grain boundary and crystal surface, I and Br ions will eventually agglomerate to form Br-rich and I-rich phases on the grain boundary and crystal surface. This segregation

Correspondence to: Z W Jin, jinzw@lzu.edu.cn
Received 28 DECEMBER 2020; Revised 24 JANUARY 2021.

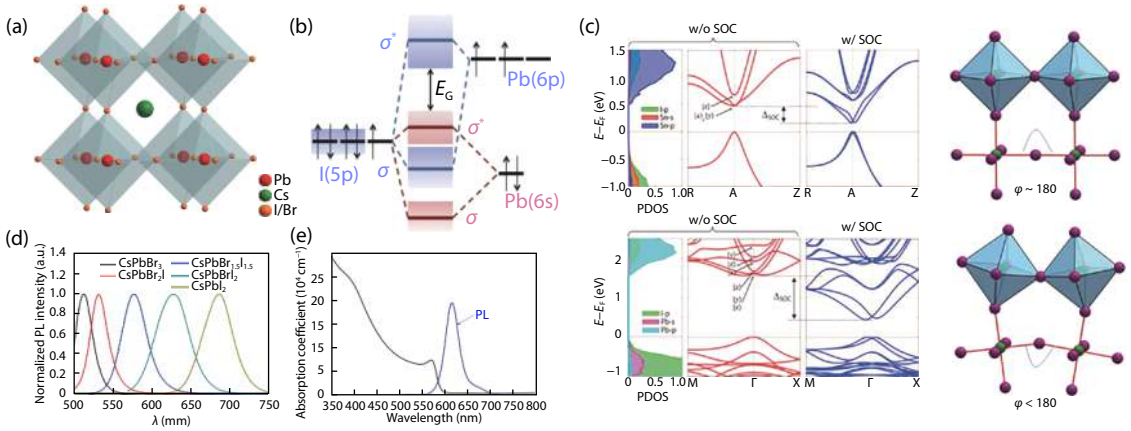

Fig. 1. (Color online) (a) Crystal structure of cubic $CsPbX_3$ perovskite. Reproduced with permission[35]. Copyright 2019, Springier Publications. (b) The mechanism of bonding/antibonding orbitals of ABX_3. Reproduced with permission[96]. Copyright 2016, American Chemical Society Publications. (c) The phase transition causes the angle of the M–X–M to decrease from 180°, leading to a change in the conduction band minimum and valence band maximum, thereby affecting the bandgap[30]. Copyright 2015, American Chemical Society Publications. (d) Absorbance spectra for inorganic perovskite films with different compositions of $CsPb(I_{1-x}Br_x)_3$. Reproduced with permission[35]. Copyright 2018, Elsevier Inc Publications. (e) Absorption coefficient and steady state PL spectrum of $CsPbBr_2I$. Reproduced with permission[22]. Copyright 2016, Wiley-VCH Publications.

has a serious impact on the photoelectric properties of mixed halides. The consequences of phase segregation are generally considered based on two aspects: (1) It results in severe current density–voltage (*J*–*V*) hysteresis, and affects the performance of the device. (2) During the migration of halide ions under light, they will be adsorbed by high-energy grain boundaries and crystal surfaces, and agglomerate on the grain boundaries and crystal surfaces. As such, grain boundaries, grains and crystal surfaces have high energy, and play an important role in ion migration. The accumulation of ions at the grain boundaries will lead to the formation of I-rich and Br-rich phases resulting in phase segregation. However, the I-rich phase (tending to 1.55 eV) and the Br-rich phase (tending to 2.3 eV) produced by phase segregation deviate from the appropriate bandgap respectively, resulting in the red shift and blue shift of absorption, affecting absorption and reducing efficiency. This is a significant reason for the PCE of $CsPbBr_2I$ being lower than that of other inorganic PSCs. However, due to the limitations of microscopic observation, the mechanism of phase segregation cannot currently be fully confirmed [26, 27].

In this review, we first introduce the crystal structure and photoelectric properties of $CsPbBr_2I$. Secondly, by analyzing the structure of $CsPbBr_2I$, the reasons for its high thermal stability and phase transition are revealed. Next, we discuss possible strategies to suppress light-induced phase transition, such as reducing the numbers of grain boundaries by improving the spin-coating of the membrane, so as to prepare a large-grain membrane, reducing the grain boundary's surface energy by modifying the interface, and changing the bonding length via ion doping. Finally, we discuss the problems in this field, and provide an outlook for the future of $CsPbBr_2I$.

2. The crystal/electronic structure and optical properties of $CsPbBr_2I$

2.1. Crystal structure

Like other $CsPbX_3$ (X = I^-, Br^-), the crystal structure of $CsPbBr_2I$ can be described as the Pb site, and X site ions form a $[MX_6]^{4-}$ corner-shared octahedron; Cs^+ is located in the center of the octahedron, as shown in Fig. 1(a)[28, 29]. Perovskite follows the Goldshmidt tolerance factor, *t*, as given in Eq. (1):

$$t = \frac{r_A + r_X}{\sqrt{2}(r_B + r_X)}, \tag{1}$$

where r_A, r_B, and r_X are the ionic radii of their respective ions in the ABX_3. With respect to $CsPbX_3$, the halide anion has a smaller negative charge than the oxide anion, and the halide ion has a large radius. This requires a large cation ion radius, and low valence at the A site, so Cs^+ is the appropriate choice for inorganic ions, and is sufficient to maintain the perovskite structure[30–33].

According to Eq. (1), when $0.8 < t < 1$, the perovskite phase structure has a relatively high PCE. When $t < 0.8$, the efficiency of the resulting non-perovskite phase is very low. In theory, by introducing other ions to tune the *t* value to between 0.9 and 1, we could increase the stability of $CsPbBr_2I$.

2.2. Electronic structure

The electronic structures of different components of $CsPbX_3$ share great commonalities. The valence band maximum (VBM) of $CsPbBr_2I$ is primarily composed of anti-bonding hybrid Pb 6s, and X np (X = I^-, Br^-) orbitals, where the main contribution is X np. The conduction band minimum (CBM) is determined by the anti-bonding mixture of Pb 6p and X np orbitals, and the main contribution is Pb 6p, as shown in Fig. 1(b)[34]. In the ideal undistorted perovskite crystal structure, the axial orbital overlap between the halide p-orbital and the metal s- and p-orbitals is optimal, and this overlap causes the s-type valence band to be significantly widened, thereby significantly increasing the bandwidth and reducing the band gap. When the phase changes from *α*-, to *β*-, to *γ*-, the octahedral structure begins to tilt, and the axial orbital coincidence decreases, resulting in a decrease in the bandwidth, an increase in the bandgap, and an increase in the density-of-states (DOS) at the top of the valence band, as shown

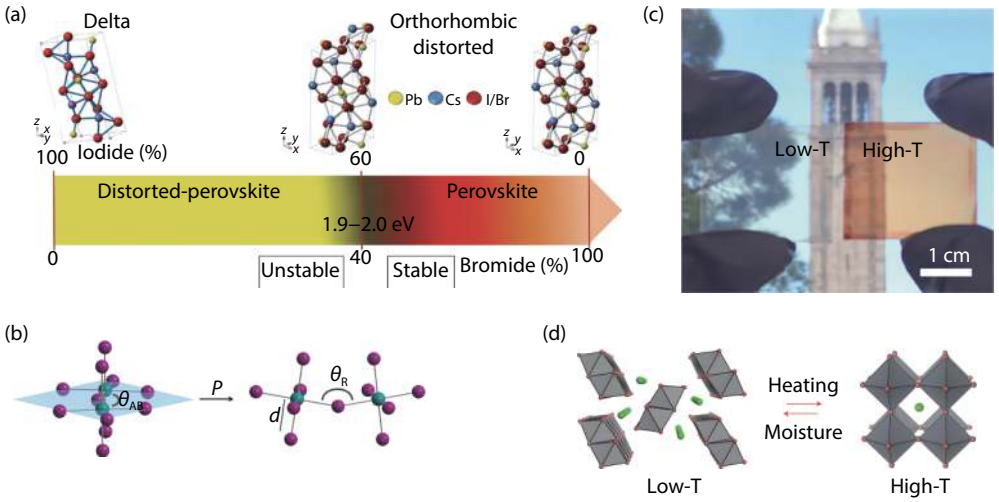

Fig. 2. (Color online) (a) Illustration depicting the perovskite crystal structure as a function of the iodine/bromine ratio. Reproduced with permission[40]. Copyright 2018, Wiley-VCH Publications. (b) The phase transition causes the angle of the M-X-M to decrease from 180° due to the influence of temperature. Reproduced with permission[31]. Copyright 2016, American Chemical Society Publications. (c) Photograph of the low-T phase (non-coloured) and high-T phase (orange-red-coloured) thin films. Reproduced with permission[45]. Copyright 2018, Nature Publications Group. (d) The low-T phase is represented by one-dimensional chains of edge-sharing lead-halide octahedra, whereas in the high-T phase, the octahedra share corners. Reproduced with permission[45]. Copyright 2018, Nature Publications Group.

in Fig. 1(c)[30].

2.3. Optical properties

The optical properties of $CsPbBr_2I$ are described in terms of absorption and quantum yield (QY).

(1) Fig. 1(d) shows that as the iodine concentration increases, the wavelength becomes longer, and the absorption begins to shift[35, 36]. As Fig. 1(e) clearly shows, the absorption of the film starts at about 605 nm, corresponding to a bandgap of about 2.08 eV[37, 38].

(2) QY is a measure of the capacity of optoelectronic devices to absorb light-emitting electrons. For a QY of $CsPbX_3$ between 10%–90%, Samanta *et al.* measured the fluorescence QY of $CsPbBr_3$ and $CsPbBr_2I$ to be ~40% and ~10%. This indicates the presence of many inherent trap states in $CsPbBr_2I$, which affect the low-emission intensity. The main trapping states result from iodine-induced distortion of the corner sharing $[Pb(Br/I)_6]$ octahedral of the cubic $CsPb(Br/I)_3$ nanocrystals, leading to the formation of a twisted crystal structure[39].

3. Phase transition of all-inorganic halide perovskite

Stability is a major challenge for all inorganic $CsPb(I_{1-x}Br_x)_3$ ($0 \leqslant x \leqslant 1$); this includes both thermal stability and optical stability. The stability of $CsPb(I_{1-x}Br_x)_3$ is dependent on the ratio of Br/I content. Fig. 2(a) shows that when $x > 0.2$, $CsPb(I_{1-x}Br_x)_3$ has a stable orthorhombic perovskite structure at room temperature. When $x < 0.2$, the perovskite structure tends to transform to the delta phase at room temperature, i.e., a thermally-induced phase transition, including for $CsPbI_3$[40]. This is due to the larger radius of I ions, which makes the chemical bond between I^- and Cs^+ longer, resulting in an unstable lattice with a tendency to transform into the delta phase. As such, Br, with its small radius, is an ideal ion. It matches the radius of Cs^+, leading to the formation of a more stable crystal structure[41].

However, with an increase in the Br/I content, the thermal stability of the material is generally overcome, while the optical stability of the material gradually weakens, i.e., light-induced phase segregation. When $x > 0.2$, phase segregation occurs under light, which specifically manifests as a large number of I ions gathering at grain boundary or grain surface to form a compound, resulting in lower cell efficiency. This is primarily because mixed halide anions cannot exist uniformly in the lattice, due to ionic radius and electronegativity problems. When the external light provides energy, the two kinds of ions tend to segregate[42].

Taking into account the above two issues, the Br/I ratio in $CsPbBr_2I$ determines its characteristic of strong thermal stability, but also causes phase segregation under illumination. In the following section, we will first analyze the thermal stability mechanism of $CsPbBr_2I$, then discuss the internal causes of severe phase segregation in $CsPbBr_2I$, and finally provide some strategies to prevent phase segregation.

3.1. Thermally induced phase transition

For the all-inorganic version, a substantial change in the crystal structure, namely phase transition, will occur at different temperatures. Phase transition is the transition between different crystal lattices and it is accompanied by the absorption or release of heat. In this part, we first discuss the mechanism of thermally induced phase transition, and then elaborate the phase transition of $CsPbBr_2I$.

3.1.1. Mechanism of thermally induced phase transition

A phase transition is a change in the crystalline structure of the same substance at different temperatures. Each crystal structure at different temperetures is known as a phase. Since different crystal structures have different optical properties and cell parameters, perovskite materials have different light absorption rates at different temperatures, with the result that different efficiencies are produced under different phases[43, 44]. The root cause of perovskite phase transition is that the perovskite skeleton is a double bridge connecting hal-

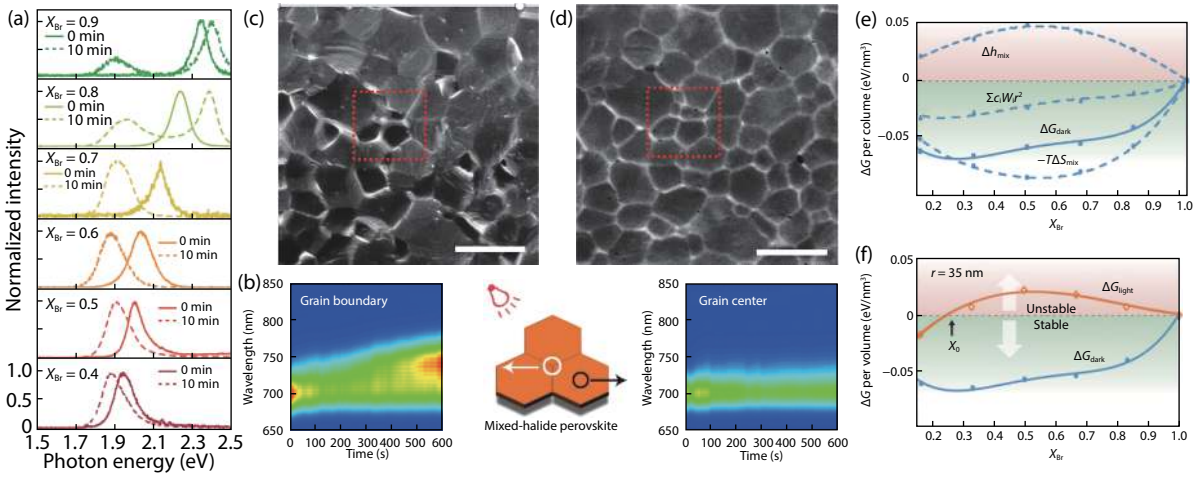

Fig. 3. (Color online) (a) The photoluminescence peak of these mixed-halide perovskites shifted exclusively to 1.87 eV after continuous illumination. The solid lines denote the spectra taken from freshly made samples, and the dashed lines dentote the measurements following 10 min illumination at an intensity of 0.3 W/cm^2. Reproduced with permission[56]. Copyright 2019, Nature Publications Group. (b) Ion migration diagram of $CsPb(I_{1-x}Br_x)_3$ in the grain interior and at the grain boundary under light. Reproduced with permission[53]. Copyright 2018, American Chemical Society Publications. (c) Secondary electron SEM image of $CsPbBr_2I$ film surface. (d) CL mapping of the $CsPbBr_2I$ film. Reproduced with permission[52]. Copyright 2017, Wiley-VCH Publications. (e) The calculated ΔG_{dark} per volume (solid line) is negative, regardless of the Br content. (f) Under illumination, as the grain size exceeds X_0, $\Delta G_{light} > 0$. Reproduced with permission[56]. Copyright 2019, Nature Publications Group.

ide ions (M–X–M moiety), as shown in Fig. 2(b)[30]. Under the influence of external temperature or pressure, the perovskite reduces the symmetry by changing the angle of M–X–M to adapt to the corresponding external conditions.

3.1.2. $CsPbBr_2I$ thermally-induced phase transition

The crystal structure of $CsPbBr_2I$ is mainly high-temperature (α-perovskite), inculding the space group Pm-3m, and the low-temperature non-perovskite phase (δ-perovskite), Pmnb[45]. The high-temperature phase has a deep orange color, and the low-temperature phase is nearly lucent, with a low PCE, as shown in Fig. 2(c). In the process of preparing $CsPbBr_2I$, the halide is heated above the temperature at which the low-temperature phase changes to the high-temperature phase, resulting in the formation of a high-temperature phase.

In an inert environment, with a decrease in temperature, the high-temperature phase forms a metastable state, and remains at room temperature, thereby maintaining extremely high efficiency. As shown in Fig. 2(d), the transition from the high-temperature to the low-temperature phase is reversible. However, for $CsPbI_3$, after about 320 °C heating and cooling, a high-temperature metastable phase forms at room temperature, and heating the metastable phase again causes it to transform extremely easily into a low-temperature non-perovskite phase. As the I^- on the $CsPb(I_{1-x}Br_x)_3$ ($0 \leqslant x \leqslant 1$) lattice is partially replaced with Br^-, the bromine-rich crystal structure has a more suitable t, and is not prone to thermodynamic phase transition[46, 47]. For example, once the formation of $CsPbBr_2I$ forms a high-temperature metastable phase, heating within the melting point range does not readily transform into the non-perovskite phase.

3.2. Light-induced phase transition

Unlike monocrystalline silicon solar cells, $CsPbBr_2I$ halide perovskite is composed of different anions, and the migration of these anions requires relatively low energy. When there is ambient light to provide energy, ion migration will occur, and anions will migrate. In this section, we discuss the phase-segregation phenomenon of $CsPbBr_2I$ under light.

3.2.1. The origin of photo-induced phase segregation

Although newly-prepared $CsPb(I_{1-x}Br_x)_3$ ($0 < x < 1$) halide is evenly mixed, with an increase in Br content, it will display a red-shifted photoluminescence peak, which splits into two smaller peaks with different absorption wavelengths under illumination, as shown in Fig. 3(a)[48, 49]. Under light, the $CsPb(I_{1-x}Br_x)_3$ ($0 < x < 1$) mixed with halide changes from a regular arrangement to a segregation of I^- and Br^-, where the bandgap with a previously uniform halide mixture increases in the Br-rich region, and decreases in the I-rich region, respectively. In the presence of an I-rich phase, the carrier is captured and thermalized rapidly on encountering an I-rich region with low bandgap, when it is diffused by light. The I-rich phase and the homogeneous phase can also form a built-in electric field, which accelerates the sweep of carriers into the I-rich phase, leading to the formation of new defects at the grain boundary and crystal surface, which results in a decrease in fill factor, affecting the voltage and current density, and thus the overall PCE[50, 51]. This segregation exists in the grain boundary, and also in the crystal interior; however it is more prevalent at grain boundaries than inside the crystal, as shown in Fig. 3(b).

Like most $CsPb(I_{1-x}Br_x)_3$ ($0 < x < 1$) perovskites, regardless of the $CsPbBr_2I$ spin-coating methods, there is a large difference between the forward sweep and the reverse sweep voltage, resulting in a very low average voltage. This is due to I^- and Br^- agglomeration at the grain boundary and crystal surface, respectively, under light, which causes phase segregation of $CsPbBr_2I$, resulting in severe hysteresis and low efficiency. Li *et al.* first used scanning electron microscopy (SEM) and cathodoluminescence (CL) to conduct microscopic analyses of $CsPbBr_2I$[52]. Figs. 3(c) and 3(d) show the microscopic

grain morphology of $CsPbBr_2I$ under SEM and CL, respectively. The team also reported the phenomenon of "clusters" of halide I segregation at the grain boundaries and on the surface of the film[53].

3.2.2. The mechanism of photo-induced phase segregation

The study of hybrid halide perovskite ion migration has a history of more than 30 years. As for how the halide phase is segregated, although it still cannot be observed with specific equipment, some studies have found that ion migration triggers phase segregation[54, 55]. The segregation of halide ions is generally related to crystal defects, the bonding method between halides, and the formation energy required for ion migration. A great deal of research has been devoted to an understanding of the basic electronic processes of the halide hybrid system, establishing thermodynamic models, and simulating the occurrence of this phenomenon by means of theoretical calculations. Here, we introduce two typical theoretical explanations of phase separation:

(1) Nucleation theory. In this model, whether the phases of the mixed halide are uniform or segregated depends on the Gibbs free energy, ΔG. When $\Delta G < 0$, the phase of the $CsPbBr_2I$ mixed halide is stable. When $\Delta G > 0$, the mixed halide will be unstable inside the lattice, creating a driving force that segregates the halide components, and the I^- and Br^- inside the lattice will tend to separate. The Gibbs free energy in the dark (ΔG_{dark}) is a function of the average grain size, r, the temperature, T, and the relative content of bromine in the mixed halide phase, X_{Br}, as shown in Eq. (2)[56]:

$$\Delta G_{dark}(X_{Br}, T) = \frac{4}{3}\pi r^3\left[\Delta h_{mix}(X_{Br}, T) - T\cdot\Delta s_{mix}(X_{Br}, T)\right] - \sum_i c_i W_i r^2. \quad (2)$$

In the above equation, Δh_{mix} is the volumetric enthalpy, $T\cdot\Delta s_{mix}$ is the volumetric entropy, and $\Sigma_i c_i W_i r^2$ denotes the cohesive energies.

Using density functional theory (DFT) calculations, we find that, regardless of the size of the crystal grains, the ΔG is negative for any content of X_{Br} in the dark, which proves that the phase of the mixed halide is stable under dark conditions, as shown in Fig. 3(e). While light-induced polarons are introduced under illumination, polarons can generate lattice strain energy by lengthening or shortening the chemical bond between the Pb-site and the halogens, and the Gibbs free energy (ΔG_{light}) of the mixed phase under illumination depends on the lattice strain energy ($\Delta g_s > 0$) originating from the light-induced polaron and ΔG_{dark}. Because $\Delta g_s > 0$, according to Eq. (3), when the grain size, r, is large enough, the ΔG_{light} will be greater than zero under light, meaning that a driving force of phase separation will be generated, so that the mixed halide will exhibit phase separation under light. Br^-- and I^--rich domains are formed by dispersing and mixing the halide phase, as shown in Fig. 3(f):

$$\Delta G_{light}(X_{Br}, T) = \Delta G_{dark}(X_{Br}, T) + \frac{4}{3}\pi r^3\cdot\Delta g_s(X_{Br}). \quad (3)$$

However, the assumption above assumes that the temperature in the dark is the same as the temperature under light. In fact, the presence of light will inevitably cause the temperature to rise.

(2) Alloy lattice distortion theory. The serious segregation of mixed halides can be explained in the context of two mixed halide anions, which can be regarded as $A_{1-x}B_x$ alloys[57]. The two alloy components are inherently less stable, due to compatibility issues, and the ions exhibit lattice distortion due to their different radii. Crystal defects, together with the instability of the composition, make it easier for the relatively small ion-radius I^- to migrate under light excitation; compared to the interior of the crystal, the crystal surface and grain boundary have higher energy, due to lattice mismatch, and the grain boundary will adsorb a lot. The halide ions gather around the grain boundaries to form "clusters," in a process referred to as phase segregation. Phase segregation and ion migration primarily affect the hysteresis of current density and voltage. We can use the hysteresis index (HI) to describe the hysteresis of $CsPb(I_{1-x}Br_x)_3$ ($0 < x < 1$). The specific formulas are as given in Eq. (4):

$$\text{Hysteresis index (HI)} = \frac{PCE_{reverse} - PCE_{forward}}{PCE_{reverse}}. \quad (4)$$

Li *et al.* pointed out that the hysteresis index of $CsPbBr_2I$ could be as high as 43.8%, far higher than for $CsPbI_3$ or $CsPbI_2Br$. In order to reduce the hysteresis of $CsPbBr_2I$, and improve the efficiency of devices in which it is utilized, in this work, we focus primarily on methods of suppressing phase segregation, thereby reducing the hysteresis.

4. Suppressed phase segregation of $CsPbBr_2I$

In summary, the light stability of halide materials is the main obstacle to the development of $CsPb(I_{1-x}Br_x)_3$ ($0 < x < 1$) PSCs, represented here by $CsPbBr_2I$. Based on studies of the phase-segregation mechanism, we believe that phase segregation must be suppressed at the grain boundary, the film surface, and the lattice interior.

(1) For grain boundaries, a film with large grains and few grain boundaries can be prepared by improving the preparation method.

(2) For the surface of the film, serial passivation can be used to reduce the surface energy and suppress ions' bias polymerization.

(3) For the inside of the grain boundary, ion doping can be used to enhance bonding, which effectively inhibits the ion migration caused by lattice expansion due to photo-generated carriers.

These three strategies for phase segregation suppression are described in detail below.

4.1. Preparation of large grain film

The defects on the perovskite film and numerous grain boundaries possess high energy; when halide ions migrate under light, these defects will adsorb halide ions, causing halide ions to agglomerate, and phase segregation to occur. As such, the preparation of perovskite films with large grains, no pinholes, and no cracks is key to suppressing phase segregation and obtaining high PCE for perovskite devices[58, 59]. In order to prepare a more ideal perovskite film, researchers generally optimize the film's morphology using one of two approaches:

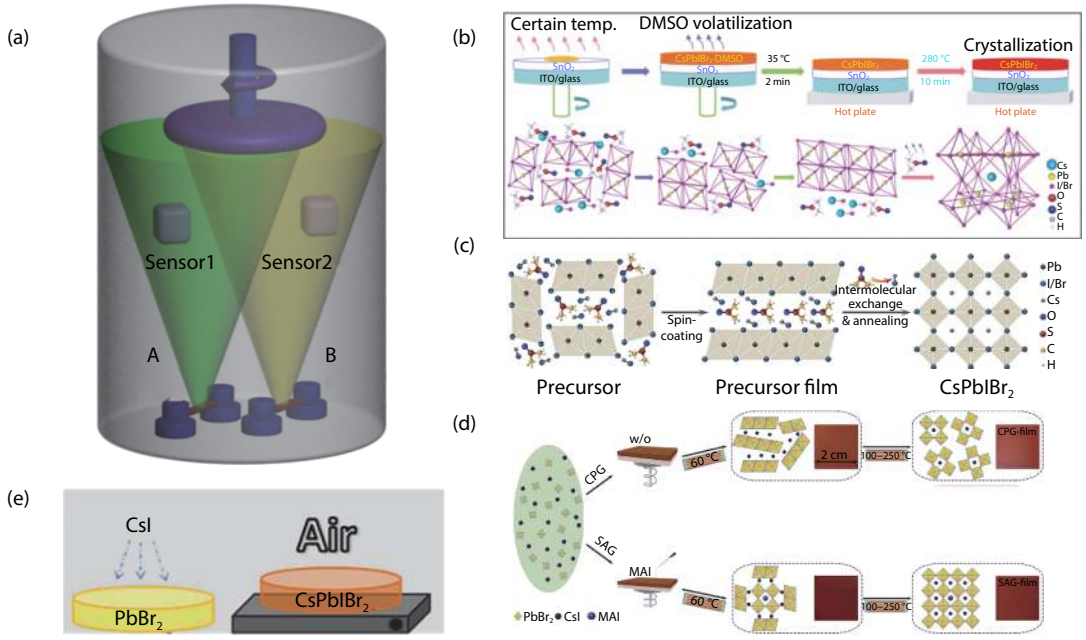

Fig. 4. (Color online) (a) Schematic diagram of dual-source thermal evaporation. Reproduced with permission[97]. Copyright 2018, Wiley-VCH Publications. (b) Illustration of $CsPbBr_2I$ perovskite film, fabricated using a preheating-assisted spin-coating process. Reproduced with permission[62]. Copyright 2019, The Royal Society of Chemistry. (c) Illustration of intermolecular exchange strategy. Reproduced with permission[59]. Copyright 2018, Wiley-VCH Publications. (d) Schematic illustration of conventional pathway growth (CPG), and seed-assisted growth (SAG) methods. Reproduced with permission[63]. Copyright 2020, Wiley-VCH Publications. (e) Illustration of $CsPbBr_2I$ film with spray-assisted deposition. Reproduced with permission[65]. Copyright 2016, American Chemical Society Publications.

(1) The continuous exploration and improvement of film preparation methods has led to developments in spin-coating-based methods, and includes other film preparation methods such as the doctor blade, inkjet-printing, and slot-die coating for film preparation[60].

(2) Optimization of the technology under different preparation methods, such as annealing temperature and time, the composition of the solvent, and the modification of some intermediates.

Combining the two approaches above, we have improved the traditional film preparation methods and preparation processes, and developed new $CsPbBr_2I$ spin-coating methods, which have continuously improved solar cell efficiency. In the next section, we investigate traditional spin-coating methods, and examine the improved processes for each type of film[61].

4.1.1. Dual source thermal evaporation

The first $CsPbBr_2I$ film was first prepared using the dual source thermal evaporation method; as shown in Fig. 4(a), its efficiency reached 4.7%. This method can be used for large-scale production and coating in industry. The process involves loading CsI and $PbBr_2$ into the device with a 1 : 1 ratio, heating of the two substances to a predetermined temperature, and evaporating to the preheated TiO_2 substrate to prepare the $CsPbIBr_2$ sample.

Since the entire spin-coating process is carried out in steam, there is no residual liquid on the substrate, and the thickness of the film can be controlled by controlling the spraying rate[22]. However, the main issue of dual-source thermal evaporation is that CsI and $PbBr_2$ will sublime on the TiO_2 substrate at high temperatures, resulting in an uneven film. Furthermore, the annealing temperature and the substrate temperature will also affect the quality of the film. Therefore, the production of high-efficiency $CsPbBr_2I$ films is not possible using this method.

4.1.2. One-step method

The traditional one-step method is to dissolve CsI and $PbBr_2$ dimethyl sulfoxide (DMSO) in a 1 : 1 ratio, spin-coating them onto a TiO_2/SnO_2 substrate, and annealing to obtain a $CsPbIBr_2$ film. Although the one-step method is extremely easy to operate, it has many shortcomings, such as poor solubility of Br^- in the solution, resulting in uneven film composition, lattice defects, and a reduction in the quality of the film. In addition, DMSO combines with $PbBr_2$, forming a complex $PbBr_2$-DMSO intermediate, which prevents the crystallization of $CsPbBr_2I$ film, and results in isolated holes on the film[58].

In order to overcome these problems, Que *et al.* preheated the substrate prior to spin-coating, which resulted in improved film coverage, as shown in Fig. 4(b), where the resulting grain size is 0.2–2 μm. However, the preheating temperature of the substrate is not easy to control. If the preheating temperature is too high, disorder in the $[Cs\text{-}PbBr_2]^+$ arrays in the initial formation will cause frost on the film's surface, and have an impact on overall device performance. Zhu *et al.* used the method of intermolecular exchange to prepare their $CsPbBr_2I$ film, as shown in Fig. 4(c). The method involves a precursor $CsPbBr_2I$ film, prepared according to the one-step method, which is then coated onto the TiO_2 substrate. For the intermolecular exchange, a methanol solution containing CsI is spin-coated onto the $CsPbBr_2I$ precursor film, then washed with anhydrous IPA (isopropanol). After annealing, the resulting $CsPbBr_2I$ film exhibited long-term stability and a greatly improved efficiency as compared to the traditional one-step method[62].

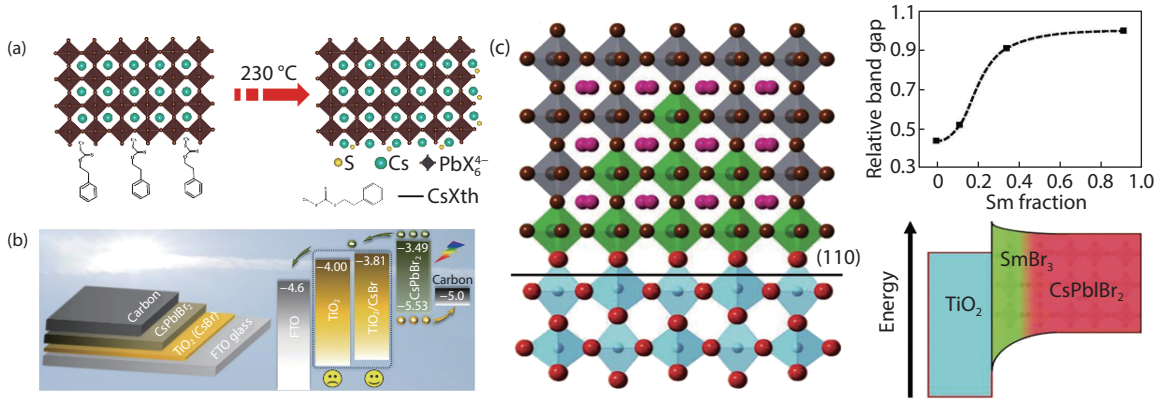

Fig. 5. (Color online) (a) Illustration of CsXth decomposition, and sulfur doping in perovskite. Reproduced with permission[72]. Copyright 2019, Elsevier Inc Publications. (b) Schematic architecture of the cell, together with the corresponding energy band diagrams for TiO_2 and TiO_2/CsBr ETLs. Reproduced with permission[73]. Copyright 2019, Wiley-VCH Publications. (c) $SmBr_3$ doping normalizes the gap between $CsPbBr_2I$ and TiO_2. Reproduced with permission[74]. Copyright 2019, Wiley-VCH Publications.

Whether employing a one-step method, preheating assisted deposition, or intermolecular exchange, since the formation of $CsPbBr_2I$ crystals requires high formation energy, high-temperature annealing can result in the growth of large grains, which increases production costs, and limits its application in flexible devices. In order to reduce the formation energy of $CsPbBr_2I$ crystals to lower the annealing temperature, Zhang *et al.* treated their $CsPbBr_2I$ film with methylammonium halides (MAX, X = I, Br) prior to annealing, so that the MA^+ was at the center of the $CsPbBr_2I$ crystal nucleation, thereby greatly reducing its formation energy, meaning that the final annealing temperature could be reduced to 150 °C[63]. As shown in Fig. 4(d), compared with a $CsPbBr_2I$ film synthesized by the conventional route, the color of the film after MAX treatment becomes noticeably darker, and its absorbance is improved.

4.1.3. Two steps method

Given that, in the one-step method, the solubility of Br^- in the precursor solution is relatively small, and ion doping is difficult, a two-step method has been proposed to resolve this difficulty. This primarily consists of dissolving $PbBr_2$ in N, N-dimethylformamide (DMF) and DMSO as a precursor solution, and spinning it on the substrate, followed by drying on the heating stage for a period of time. The prepared film is then immersed in a methanol solution of CsI for a period of time, before being annealed to obtain a $CsPbBr_2I$ film with an efficiency of 8.25%[64]. However, the disadvantage of this method is that it results in the presence of residual methanol solution on the substrate, which affects the crystallization of the film. In order to further improve efficiency and film production speed, Lau *et al.* initially spin-coated a precursor solution of $PbBr_2$ onto a mesoporous TiO_2 substrate. The difference from the two-step method is that the methanol CsI solution forms steam at high temperatures, which is then sprayed onto the precursor film, and annealing for a period of time causes the film to crystallize in air, as shown in Fig. 4(e)[65]. For better control of the annealing temperature and in order to grow large-grain films, Wang *et al.* developed a two-step temperature-control annealing process: having prepared their $CsPbBr_2I$ film via the two-step method, the substrates were first placed onto a hotplate at a temperature of 150 °C for about 10 min. The substrates were then placed onto the hotplate at a temperature of 280 °C for 10 min. Using this method, the highest PCE achieved was 8.31%, as compared with the one-step PCE of 4.98%, an efficiency increase of 66.9%[66].

Having discussed the basic spin coating method and its improvements above, we find that each method has certain drawbacks, and that some process parameters are not ideal, such as the annealing temperature, substrate temperature, annealing time, spray rate, etc. All in all, making perovskite films with few defects and large grains helps reduce hysteresis and improve efficiency.

4.2. Passivation of film surface

Halide phase segregation will generate a large number of mobile ions near the grain boundaries or inside the crystal grains of the $CsPbBr_2I$ film. These mobile ions accumulate near the $CsPbBr_2I$/ETL interface to form an incident electron injection barrier, which is not conducive to small extraction[60, 67, 68]. Therefore, the selection of appropriate charge transfer materials or materials to modify the $CsPbBr_2I$/ETL interface could effectively reduce hysteresis and improve efficiency. At the same time, the choice of modifier to modify the interface may result in a better match in the band between $CsPbBr_2I$ and ETL, further reducing the energy loss[69]. With respect to charge transport materials, TiO_2, SnO_2, In_2S_3, etc., are generally selected[70].

(1) TiO_2 is the most widely-used charge transport material, but its disadvantages include higher sintering temperature, narrow band gap, and relatively low electron mobility[71]. In order to improve the charge extraction rate of the $CsPbBr_2I$/ETL interface, thereby improving efficiency, Hayase *et al.* used Xanthate to coat the surface of the $CsPbBr_2I$; this then decomposed into S^{2-} following high-temperature annealing, as shown in Fig. 5(a). Since S^{2-} has a strong chemical bond with perovskite, which interacts with the perovskite phase, the perovskite film surface is passivated and stablised for a long time[72]. Zhu *et al.* used CsBr clusters to modify the TiO_2 interface. Their study found that CsBr changed the CBM of TiO_2, increasing it from –4.00 to –3.81 eV, while at the same time reducing the TiO_2 power function from 4.11 to 3.86 eV[73]; Fig. 5(b) shows the band alignment diagram following this modification. CsBr clusters can also play a role in nucle-

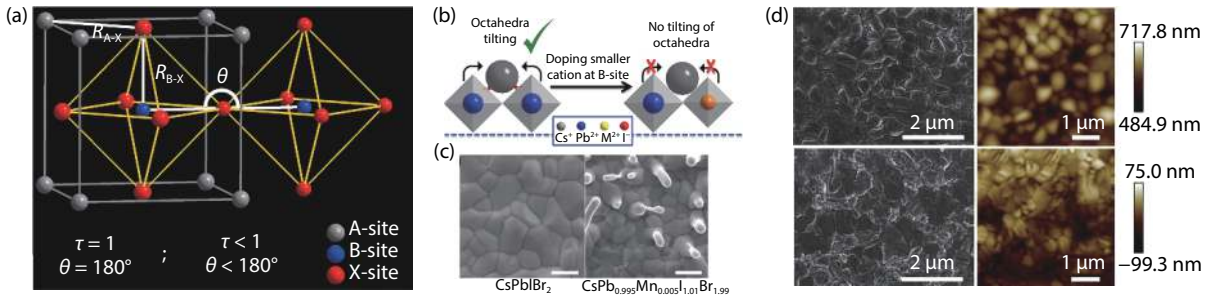

Fig. 6. (Color online) (a) Relation of the tolerance factor (τ) with a B–X–B bond angle (θ) of the ABX_3 perovskite structure. Reproduced with permission[88]. Copyright 2018, American Chemical Society Publications. (b) Rotational distortion of $[BX_6]^{4-}$($[PbX_6]^{4-}$) octahedra can be restricted by reducing the B–X bond length when Pb^{2+} is partially substituted with smaller B-site cations. Smaller B-site cations reduce the size of the $[BX_6]^{4-}$ octahedron, which in turn decreases the size of the cuboctahedral void for the A-site cation. Reproduced with permission[88]. Copyright 2018, American Chemical Society Publications. (c) Typical SEM images of $CsPbBr_2I$, and $CsPb_{0.995}Mn_{0.005}Br_{1.99}I_{1.01}$ films, respectively. Reproduced with permission[91]. Copyright 2018, Wiley-VCH Publications. (d) SEM images of (above) $CsPbBr_2I$ and (below) $CsPb(Ba)Br_2I$. Reproduced with permission[93]. Copyright 2017, Elsevier Inc Publications.

ation, promoting interface nucleation to improve efficiency. Liu *et al.* used $SmBr_3$ to suppress phase separation[74]. The mechanism here is that Sm and TiO_2, in combination with $SmBr_3$, form Ti–O–Sm, thereby enhancing the interface. Moreover, Sm can replace Pb to permit gradient band doping, as shown in Fig. 5(c). The results show a reduction in HI, from 15.1% to 6.6%, while efficiency remained stable at about 10%.

(2) $CsPbBr_2I$ film produced with SnO_2 as the transport layer has high crystallinity and extremely uniform crystal grains, but the opening voltage is relatively low, while TiO_2 is conducive to the separation and extraction of charges[75]. Exploiting the advantages of both methods, Cao *et al.* found that depositing a TiO_2 atomic layer onto SnO_2 can significantly improve the PCE of carbon-based all-inorganic perovskites. A TiO_2 layer on an SnO_2 electron transport layer simultaneously boosts the crystallization and increases grain size. The charge extraction and transportation are also effectively improved[76].

(3) In addition to the above two methods, ZnO and In_2S_3 can also be used as ETL transport layers for $CsPbBr_2I$[77]. For both are stable and non-toxic to In_2S_3, and both possess a wide energy band, with greater carrier recombination than TiO_2[78]. Yang *et al.* found that the efficiency of In_2S_3 is significantly greater than that of TiO_2 under the same conditions, making it an ideal transport material[79].

4.3. Doping increases bond strength

Doping could introduce other ions into the crystal lattice, altering the crystal structure to suppress phase segregation and improve the performance of the material[80–82]. Doping has three main effects in terms of suppressing phase segregation.

(1) Increasing bonding strength. Since light can cause the crystal lattice of $CsPbBr_2I$ to stretch which in turn causes phase segregation, we can introduce ions with strong bonding close to the Cs^+ and Pb^{2+} sites to partially replace the A site or the B site, thereby altering the bonding strength and distance of A–X and B–X, as shown in Fig. 6(a). If the bonding between A–X and B–X is enhanced, the photo striction can be reduced, thereby suppressing phase segregation[83].

(2) Improving the crystallinity of the material. Pinhole defects in $CsPbBr_2I$ films are the main sites of ion migration induced by phase segregation[84, 85]. Doping can participate in the crystallization process, increase the crystallinity of the film, and shorten the crystallization time, thereby resulting in a more regular film, in order to suppress phase segregation.

(3) Changing the optical and electronic performance. Because phase separation occurs under light, doping can change the band gap by changing the CBM and VBM of $CsPbBr_2I$, thereby affecting the light absorption of $CsPbBr_2I$, which essentially inhibits phase separation.

By summarizing the effects of doping, we can then analyze the effect of doping on $CsPbBr_2I$ performance from A site and B site, respectively.

4.3.1. A-site doping

In $CsPbBr_2I$, the Cs^+ at the A site determines the space size of the corner-sharing $[PbBr_6]^{4-}$ octahedra, and the introduction of ions with an A radius greater than Cs, such as (FA or MA), or ions less than Cs^+, can inhibit phase segregation. Its main effect is to reduce lattice distortion caused by excited carriers through the substitution of other A-site ions, which promotes the thermodynamic stability of the uniform phase, and inhibits segregation[86]. Tan *et al.* incorporated Li into the A site of $CsPbBr_2I$; compared with non-doped devices, the efficiency was increased by 1.84%[87]. This is because the introduction of Li^+ into the crystal lattice of $CsPbBr_2I$ resulted in an increase in bond strength between the Cs, Pb, and halides, which helped to inhibit phase separation, and in addition, the average grain size of the crystals obtained via Li^+ doping was significantly larger than that of undoped crystals.

4.3.2. B-site doping

With regard to B-site doping, the optical characteristics are mainly affected by CBM and VBM. Therefore, a partially-doped metal site (B-site cation) is a more direct and effective way to change the effect of photo striction on light illumination, and may eliminate the phase segregation problem[88]. The choice of B-site dopant and its main mechanism is illustrated in Fig. 6(b). In addition, compared with undoped $CsPbBr_2I$, doped $CsPbBr_2I$ film has a better coverage.

Given that the energy level of B-site Pb is relatively deep, B-site doping with other metal ions may cause new deep defects, which will serve as scattering centers to further affect the original photoelectric properties of $CsPbBr_2I$[78]. Therefore,

Table 1. Perovskite structure, preparation techniques, and device performance for all reported variants.

Optimization strategy	Perovskite structure	Perovskite fabrication method	V_{OC} (V)	J_{SC} (mA/cm^2)	FF (%)	PCE (%)	Ref.
Spin coating method	Glass/FTO/c-TiO_2/$CsPbBr_2I$/Au	Dual source evaporation	0.959	8.7	0.56	4.7	[22]
	ITO/SnO_2/$CsPbBr_2I$/Spiro-OMeTAD/Ag	Preheating assisted spin-coating	1.267	10.69	0.71	9.86	[62]
	FTO/c-TiO_2/$CsPbBr_2I$/Carbon	One-step spin coating	1.171	9.01	0.52	5.49	[58]
		Intermolecular exchange	1.245	10.66	0.69	9.16	[59]
	FTO/SnO_2/$CsPbBr_2I$/Spiro-OMeTAD/Au	Seed-assisted growth	1.21	11.94	0.73	10.47	[63]
	Glass/FTO/bl-TiO_2/c-TiO_2/$CsPbBr_2I$/Spiro-OMeTAD/Au	Spray assisted deposition	1.121	7.94	0.7	6.3	[65]
Interface modification	ITO/SnO_2 NPs/$CsPbBr_2I$/CsXth/P3HT/Au	One-step spin coating	1.3	10.19	0.738	9.78	[72]
	FTO/TiO_2(CsBr)/$CsPbBr_2I$/Carbon	Intermolecular exchange	1.261	11.8	0.72	10.71	[73]
	FTO/TiO_2/$SmBr_3$/$CsPbBr_2I$/Spiro-OMeTAD/Au		1.17	12.75	0.73	10.88	[74]
	FTO/SnO_2/TiO_2/$CsPbBr_2I$/carbon		1.273	10.91	0.66	9.31	[75]
	ITO/In_2S_3/$CsPbBr_2I$/Spiro-OMeTAD/Ag	One-step spin coating	1.09	7.76	0.66	5.59	[79]
	Glass/FTO/ZnO/$CsPbBr_2I$/Carbon		1.03	11.6	0.63	7.6	[78]
	Glass/FTO/c-TiO_2/Li-$CsPbBr_2I$/CuPc/Carbon		1.22	10.27	0.74	9.25	[87]
Ion doping	FTO/c-TiO_2/m-TiO_2/$CsPb_{0.995}Mn_{0.005}Br_{1.99}I_{1.01}$/Carbon	Two steps spin coating	0.99	13.15	0.57	7.36	[91]
	FTO/c-TiO_2/m-TiO_2/$CsPb_{0.9}Sn_{0.1}Br_2I$/Carbon		1.26	14.3	0.63	11.33	[64]
	Glass/FTO/c-TiO_2/CsPb(Ba)Br_2I/Spiro-OMeTAD/Au	One-step spin coating	1.19	11.91	0.74	10.51	[93]

it is very important to choose appropriate elements to replace Pb. Below are three different types of B-site doping:

(1) Among other kinds of perovskite doping, Mn^{2+} doping has proved to be an effective method to adjust the electronic and optical properties of semiconductor nanocrystals[89, 90]. As such, replacing Pb^{2+} with part of Mn^{2+} is considered to generally improve the efficiency of $CsPbBr_2I$. Liang *et al.* synthesized a new Mn-doped all-inorganic perovskite, $CsPb_{1-x}MnxBr_{2-2x}I_{1+2x}$. When the Mn^{2+} doping concentration $x = 0.005$, Compared with the $CsPbBr_2I$ film without Mn^{2+}, the $CsPb_{0.995}Mn_{0.005}Br_{1.99}I_{1.01}$ film displays vertical branches on its surface[91]. These branches expand the contact area between the perovskite and the electrode, and promotes holes from the perovskite layer, transferred to the electrode, as shown in Fig. 6(c).

(2) Sn doping in organic–inorganic lead-halide perovskites can narrow the bandgap and achieve high cell efficiency. Li *et al.* used the one-step antisolvent method to prepare $CsPb_{1-x}Sn_xBr_2I$ (x = 0.00, 0.25, 0.5, 0.75, and 1.00) films with adjustable E_g between 2.04 and 1.64 eV[92]. In contrast to the above synthesis method, Liang *et al.* successfully prepared a new hybrid Pb/Sn inorganic perovskite $CsPb_{0.9}Sn_{0.1}Br_2I$ via a simple liquid phase process, whereby the doping band of Sn^{2+} adjusted the bandgap to 1.79 eV, and achieved an efficiency of 11.33%[64].

(3) Ba^{2+} doping results in a $CsPbBr_2I$ film with a good crystalline morphology. Liu *et al.* partially replaced Pb in $CsPbBr_2I$ with Ba (II, IR = 135 pm), which resulted in an undesirable t of less than 0.8. Ba(II) doping improves the device efficiency to 10.51%, as compared with an efficiency of 8.4% for a film not doped with Ba^{2+}[93]. Due to the participation of Ba^{2+} doping, in the crystallization process, the crystallinity of the film is increased, resulting in many small and grains, as shown in Fig. 6(d).

Doping has achieved good results in terms of suppressing phase segregation. However, there are a series of scientific problems still to be resolved regarding doping. Issues such as whether dopants should be introduced into the crystal lattice, or just isolated on the surface, and how doping ions adjust the properties of the perovskite remain a mystery. In addition, the uniformity of the doped phase needs to be investigated by means of a high-resolution and high-sensitivity characterization method.

5. Challenges and prospects

To summarize this article, we find that the biggest advantage of $CsPbBr_2I$ is that it will not fail due to thermodynamic phase change during external temperature change; i.e., it exhibits thermal stability. Its biggest shortcoming is that phase segregation can occur on exposure to light, causing hysteresis, which seriously affects efficiency. From the perspective of film preparation and interface modification, the efficiency of $CsPbBr_2I$ still shows room for improvement. In addition, the process of transferring $CsPbBr_2I$ from laboratory to commercial use represents a significant challenge. Below, we provide a brief summary of the challenges we face in the further development of $CsPbBr_2I$, and look forward to its application prospects.

5.1. Challenges

Anti-hygroscopic. Studies have shown that unencapsulated $CsPbBr_2I$ can maintain its initial performance for up to seven days at 100 °C. $CsPbBr_2I$ has excellent thermal stability, but like other halide perovskites, $CsPbBr_2I$ is particularly hygroscopic. Although it can operate normally in an environment with normal humidity, when humidity increases, water molecules will induce a non-perovskite phase in the $CsPbBr_2I$, resulting in device failure. Currently, the main protection measures to ensure moisture resistance in perovskites consist of mineral oil with hydrophobic and sealed packaging. However, organic mineral oil is an environmental pollutant, and is not convenient to use; we therefore need to conduct

in-depth research into battery packaging materials.

Light stability. The critical issue to be addressed for $CsPbBr_2I$ is the phenomenon of light-induced segregation. Three approaches have been proposed above. It is commonly accepted that structure determines performance, given that the theoretical analysis of photo-induced segregation is based only on computer simulation calculations, and the effect of light-induced polaron on the lattice is only assumed. Therefore, the mechanism of phase segregation must be studied energetically in order to positively inhibit it.

Low PCE. Although the PCE of $CsPbBr_2I$ can be as high as 11%, compared with other Cs-based all-inorganic perovskite, its PCE is not very high. Although the bandgap determines the limited optical absorption range of $CsPbBr_2I$, maximizing its efficiency within the limited optical absorption range is an issue requiring to be addressed. At present, there is not much room for film preparation and energy band alignment, and the main focus of future research should be to introduce interface passivators or ion doping to improve efficiency.

5.2. Outlook

Third-generation perovskite photovoltaic devices are primarily being developed with an eye to energy conservation and environmental protection. In the current experimental development stage, the selection of materials used to make devices is slowly shifting towards low cost and environmental protection considerations.

Development of inexpensive electrodes. Precious metal electrodes such as Au, Ag, etc. were previously selected for use in electrodes, while for the band connection between these metal electrodes and the perovskite layer, Spiro-MeOTAD, PCBM, etc. were used. On the one hand, these materials have poor stability, and on the other hand, these materials are extremely expensive to use, and cannot be converted for commercial use. In this regard, the replacement of the above-mentioned precious metal electrodes with carbon electrodes and hole-free transport materials is imperative in the long run. However, although current perovskite batteries made with carbon electrodes exhibit stable efficiency, they are generally relatively rare. It is to be expected that in the next few years, the number of perovskite batteries utilizing carbon electrodes will increase significantly.

Study nontoxic perovskites. Since the use of toxic Pb metal in perovskite materials causes serious environmental pollution after degradation, it is necessary to develop a pollution-free alternative to the use of lead. Several less toxic or non-toxic metals (Bi, Sn, Mn, Sb and Ge) represent possible substitutes for Pb. For the purpose of future research into the replacement of lead, in theory, attention should be paid to the following two points: (1) For any candidate material to replace lead, the ionic radius should follow an ABX_3 formation of t ($0.8 < t < 1$); if the alternate radius is too large or too small, this will lead to t deviating from the ideal range, and produce poor results. (2) Pb is the main contributor to CBM and VBM, which decides the light absorption performance of perovskite materials; as such, replacement metal ions should share the same basic electronic structure as Pb. Sn is considered to be the most likely alternative to Pb metal, but the instability of Sn is also a problem worthy of our consideration. There is still a long way to go in the study of lead-free perovskites.

Explore the recyclability of ETL. TiO_2 transmission materials are widely used for ETL materials, due to their stability and efficiency. Zhu *et al.* recycled their TiO_2 glass substrate after use, then soaked and dried it in DMF for recycling[94]. In the future, we may seek out more economical and pollution-free ETL materials, or continue to strengthen the exploration of recovery processes for recoverable TiO_2 substrates. This area shows great promise.

Improve the production efficiency of film. For large-scale production, the battery area we currently make is generally within 1 cm^2. In order to make perovskite cover a larger area, the spin-coating process must be changed to facilitate mass production. For example, Wang *et al.* loaded their perovskite spin-coating liquid into a syringe, with the syringe needle switched for a brush in order to coat the perovskite, which greatly improves coating efficiency[95]. This is also the future direction of coating development.

Use in the glass coloration industry. In this review, $CsPbBr_2I$ maximizes its efficiency in the absorption range by suppressing photo-induced phase segregation. However, the inherent 2.08 eV band gap makes its theoretical maximum efficiency lower than that of most other Cs-based perovskites, so its application advantages in the field of solar cells are limited. However, $CsPbBr_2I$ can be used as color changing glass, because the high-temperature phase is orange, and the low-temperature phase is nearly colorless, due to the reversibility of the phase transformation process. In the colorless-to-orange process, only heat is required, and in the orange-to-colorless process, only water induction is needed. Therefore, compared with AgBr, the use of $CsPbBr_2I$ in color-changing glass has the advantages of low cost and easy synthesis, leading to broad application prospects in the construction and automobile industries[45].

Acknowledgements

This work was funded by the National Natural Science Foundation of China (52073131, 51902148, 61704099, 61874166, U1832149, 51801088 and 51802024), the Natural Science Foundation of Gansu Province (20JR5RA227, 20JR5RA217, 20JR5RA278), and the Fundamental Research Funds for the Central Universities (lzujbky-2020-61, lzujbky-2019-88 and lzujbky-2020-kb06).

References

[1] Wang R, Mujahid M, Duan Y, et al. A review of perovskites solar cell stability. Adv Funct Mater, 2019, 29, 1808843

[2] Wang K, Jin Z, Liang L, et al. All-inorganic cesium lead iodide perovskite solar cells with stabilized efficiency beyond 15%. Nat Commun, 2018, 9, 4544

[3] Bian H, Bai D, Jin Z, et al. Graded bandgap $CsPbI_{2+x}Br_{1-x}$ perovskite solar cells with a stabilized efficiency of 14.4%. Joule, 2018, 2, 1500

[4] Zhou H, Chen Q, Li G, et al. Interface engineering of highly efficient perovskite solar cells. Science, 2014, 345, 542

[5] Yao H, Zhou F, Li Z, et al. Strategies for improving the stability of tin-based perovskite ($ASnX_3$) solar cells. Adv Sci, 2020, 7, 1903540

[6] Miyasaka T, Kulkarni A, Kim G M, et al. Perovskite solar cells: Can we go organic-free, lead-free, and dopant-free. Adv Energy Mater, 2020, 10, 1902500

[7] Wang Q, Zhang X, Jin Z, et al. Energy-down-shift $CsPbCl_3$: Mn

quantum dots for boosting the efficiency and stability of perovskite solar cells. ACS Energy Lett, 2017, 2, 1479
[8] Duan J, Zhao Y, He B, et al. High-purity inorganic perovskite films for solar cells with 9.72 % efficiency. Angew Chem Int Ed, 2018, 57, 3787
[9] Zhang J, Bai D, Jin Z, et al. 3D-2D-0D interface profiling for record efficiency all-inorganic $CsPbBrI_2$ perovskite solar cells with superior stability. Adv Energy Mater, 2018, 8, 1703246
[10] Wang K, Jin Z, Liang L, et al. Chlorine doping for black γ-$CsPbI_3$ solar cells with stabilized efficiency beyond 16%. Nano Energy, 2019, 58, 175
[11] Swarnkar A, Marshall A R, Sanehira E M, et al. Quantum dot-induced phase stabilization of α-$CsPbI_3$ perovskite for high-efficiency photovoltaics. Science, 2016, 354, 92
[12] Liu F, Zhang Y, Ding C, et al. Highly luminescent phase-stable $CsPbI_3$ perovskite quantum dots achieving near 100% absolute photoluminescence quantum yield. ACS Nano, 2017, 11, 10373
[13] Zeng Q, Zhang X, Liu C, et al. Inorganic $CsPbI_2Br$ perovskite solar cells: The progress and perspective. Solar RRL, 2019, 3, 1800239
[14] Liu C, Li W, Zhang C, et al. All-inorganic $CsPbI_2Br$ perovskite solar cells with high efficiency exceeding 13%. J Am Chem Soc, 2018, 140, 3825
[15] Lau C F J, Zhang M, Deng X, et al. Strontium-doped low-temperature-processed $CsPbI_2Br$ perovskite solar cells. ACS Energy Lett, 2017, 2, 2319
[16] Akkerman Q A, Gandini M, Di Stasio F, et al. Strongly emissive perovskite nanocrystal inks for high-voltage solar cells. Nat Energy, 2016, 2, 16194
[17] Liang J, Wang C, Wang Y, et al. All-inorganic perovskite solar cells. J Am Chem Soc, 2016, 138, 15829
[18] Zhang X, Jin Z, Zhang J, et al. All-ambient processed binary $CsPbBr_3$-$CsPb_2Br_5$ perovskites with synergistic enhancement for high-efficiency Cs-Pb-Br-based solar cells. ACS Appl Mater Interfaces, 2018, 10, 7145
[19] Zhang C, Wang K, Wang Y, et al. Low-temperature crystallization of $CsPbIBr_2$ perovskite for high performance solar cells. Solar RRL, 2020, 4
[20] Chen W, Li D, Chen S, et al. Spatial distribution recast for organic bulk heterojunctions for high-performance all-inorganic perovskite/organic integrated solar cells. Adv Energy Mater, 2020, 10, 2000851
[21] Guo N, Zhang T, Li G, et al. HI hydrolysis-derived intermediate as booster for $CsPbI_3$ Perovskite: from crystal structure, film fabrication to device performance. J Semicond, 2017, 38, 014004
[22] Ma Q, Huang S, Wen X, et al. Hole transport layer free inorganic $CsPbIBr_2$ perovskite solar cell by dual source thermal evaporation. Adv Energy Mater, 2016, 6, 1502202
[23] Kulbak M, Gupta S, Kedem N, et al. Cesium enhances long-term stability of lead bromide perovskite-based solar cells. J Phys Chem Lett, 2016, 7, 167
[24] Zhu W, Ma W, Su Y, et al. Low-dose real-time X-ray imaging with nontoxic double perovskite scintillators. Light: Sci Appl, 2020, 9, 112
[25] Zhao Y C, Zhou W K, Zhou X, et al. Quantification of light-enhanced ionic transport in lead iodide perovskite thin films and its solar cell applications. Light: Sci Appl, 2017, 6, e16243
[26] Kang C-H, Dursun I, Liu G, et al. High-speed colour-converting photodetector with all-inorganic $CsPbBr_3$ perovskite nanocrystals for ultraviolet light communication. Light: Sci Appl, 2019, 8, 94
[27] Fang H H, Wang F, Adjokatse S, et al. Photoexcitation dynamics in solution-processed formamidinium lead iodide perovskite thin films for solar cell applications. Light: Sci Appl, 2016, 5, e16056
[28] Bodnarchuk M I, Boehme S C, ten Brinck S, et al. Rationalizing and controlling the surface structure and electronic passivation of cesium lead halide nanocrystals. ACS Energy Lett, 2019, 4, 63
[29] Tian J, Xue Q, Yao Q, et al. Inorganic halide perovskite solar cells: Progress and challenges. Adv Energy Mater, 2020, 10, 2000183
[30] Stoumpos C C, Kanatzidis M G. The renaissance of halide perovskites and their evolution as emerging semiconductors. Acc Chem Res, 2015, 48, 2791
[31] Jaffe A, Lin Y, Beavers C M, et al. High-pressure single-crystal structures of 3D lead-halide hybrid perovskites and pressure effects on their electronic and optical properties. ACS Cent Sci, 2016, 2, 201
[32] Zhang H, Xiao J, Shi J, et al. Self-adhesive macroporous carbon electrodes for efficient and stable perovskite solar cells. Adv Funct Mater, 2018, 28, 1802985
[33] Shan Q, Wei C, Jiang Y, et al. Perovskite light-emitting/detecting bifunctional fibres for wearable LiFi communication. Light: Sci Appl, 2020, 9, 163
[34] Brandt R E, Stevanović V, Ginley D S, et al. Identifying defect-tolerant semiconductors with high minority-carrier lifetimes: Beyond hybrid lead halide perovskites. MRS Commun, 2015, 5, 265
[35] Ma T, Wang S, Zhang Y, et al. The development of all-inorganic $CsPbX_3$ perovskite solar cells. J Mater Sci, 2019, 55, 464
[36] Zhang M N, Wu X, Riaud A, et al. Spectrum projection with a bandgap-gradient perovskite cell for colour perception. Light: Sci Appl, 2020, 9, 162
[37] Mondal N, Samanta A. Complete ultrafast charge carrier dynamics in photo-excited all-inorganic perovskite nanocrystals ($CsPbX_3$). Nanoscale, 2017, 9, 1878
[38] Zhang J, Hodes G, Jin Z, et al. All-inorganic $CsPbX_3$ perovskite solar cells: Progress and prospects. Angew Chem Int Ed, 2019, 58, 15596
[39] Seth S, Mondal N, Patra S, et al. Fluorescence blinking and photoactivation of all-inorganic perovskite nanocrystals $CsPbBr_3$ and $CsPbBr_2I$. J Phys Chem Lett, 2016, 7, 266
[40] Sanchez S, Christoph N, Grobety B, et al. Efficient and stable inorganic perovskite solar cells manufactured by pulsed flash infrared annealing. Adv Energy Mater, 2018, 8, 1802060
[41] Ho-Baillie A, Zhang M, Lau C F J, et al. Untapped potentials of inorganic metal halide perovskite solar cells. Joule, 2019, 3, 938
[42] Beal R E, Slotcavage D J, Leijtens T, et al. Cesium lead halide perovskites with improved stability for tandem solar cells. J Phys Chem Lett, 2016, 7, 746
[43] Marronnier A, Roma G, Boyer-Richard S, et al. Anharmonicity and disorder in the black phases of cesium lead iodide used for stable inorganic perovskite solar cells. ACS Nano, 2018, 12, 3477
[44] Zhou F, Li Z, Lan W, et al. Halide perovskite, a potential scintillator for X-ray detection. Small Methods, 2020, 4, 2000506
[45] Lin J, Lai M, Dou L, et al. Thermochromic halide perovskite solar cells. Nat Mater, 2018, 17, 261
[46] Stoumpos C C, Malliakas C D, Kanatzidis M G. Semiconducting tin and lead iodide perovskites with organic cations: Phase transitions, high mobilities, and near-infrared photoluminescent properties. Inorg Chem, 2013, 52, 9019
[47] Wang K, Li Z, Zhou F, et al. Ruddlesden–Popper 2D component to stabilize γ-$CsPbI_3$ perovskite phase for stable and efficient photovoltaics. Adv Energy Mater, 2019, 9, 1902529
[48] Knight A J, Wright A D, Patel J B, et al. Electronic traps and phase segregation in lead mixed-halide perovskite. ACS Energy Lett, 2018, 4, 75
[49] Slotcavage D J, Karunadasa H I, McGehee M D. Light-induced phase segregation in halide-perovskite absorbers. ACS Energy Lett, 2016, 1, 1199
[50] Hoke E T, Slotcavage D J, Dohner E R, et al. Reversible photo-induced trap formation in mixed-halide hybrid perovskites for photovoltaics. Chem Sci, 2015, 6, 613
[51] Xu Y, Wang M, Lei Y, et al. Crystallization kinetics in 2D perovskite solar cells. Adv Energy Mater, 2020, 10, 2002558
[52] Li W, Rothmann M U, Liu A, et al. Phase segregation enhanced ion movement in efficient inorganic $CsPbIBr_2$ solar cells. Adv En-

ergy Mater, 2017, 7, 1700946
[53] Tang X, van den Berg M, Gu E, et al. Local observation of phase segregation in mixed-halide perovskite. Nano Lett, 2018, 18, 2172
[54] Jiang J, Onwudinanti C K, Hatton R A, et al. Stabilizing lead-free all-inorganic tin halide perovskites by ion exchange. J Phys Chem C, 2018, 122, 17660
[55] Li Z, Sun Y, Yao H, et al. Intermediates transformation for efficient perovskite solar cells. J Energy Chem, 2021, 52, 102
[56] Wang X, Ling Y, Lian X, et al. Suppressed phase separation of mixed-halide perovskites confined in endotaxial matrices. Nat Commun, 2019, 10, 695
[57] Yuan Y, Wang Q, Huang J. Ion migration in hybrid perovskite solar Cells. In: Organic-Inorganic Halide Perovskite Photovoltaics. Springer, 2016, 137
[58] Guo Y, Yin X, Liu J, et al. Inorganic $CsPbIBr_2$-based perovskite solar cells: Fabrication technics modification and efficiency improvement. Solar RRL, 2019, 3, 1900135
[59] Zhu W, Zhang Q, Chen D, et al. Intermolecular exchange boosts efficiency of air-stable, carbon-based all-inorganic planar $CsPbIBr_2$ perovskite solar cells to over 9%. Adv Energy Mater, 2018, 8, 1802080
[60] Cao S, Wang H, Li H, et al. Critical role of interface contact modulation in realizing low-temperature fabrication of efficient and stable $CsPbIBr_2$ perovskite solar cells. Chem Eng J, 2020, 394, 124903
[61] Zhang Q, Zhu W, Chen D, et al. Light processing enables efficient carbon-based, all-inorganic planar $CsPbIBr_2$ solar cells with high photovoltages. ACS Appl Mater Interfaces, 2019, 11, 2997
[62] Guo Y, Yin X, Liu J, et al. Highly efficient $CsPbIBr_2$ perovskite solar cells with efficiency over 9.8% fabricated using a preheating-assisted spin-coating method. J Mater Chem A, 2019, 7, 19008
[63] Zhang W, Xiong J, Li J, et al. Seed-assisted growth for low-temperature-processed all-inorganic $CsPbIBr_2$ solar cells with efficiency over 10%. Small, 2020, 16, 2001535
[64] Liang J, Zhao P, Wang C, et al. $CsPb_{0.9}Sn_{0.1}IBr_2$ based all-inorganic perovskite solar cells with exceptional efficiency and stability. J Phys Chem Lett, 2017, 139, 14009
[65] Lau C F J, Deng X, Ma Q, et al. $CsPbIBr_2$ perovskite solar cell by spray-assisted deposition. ACS Energy Lett, 2016, 1, 573
[66] Wang C, Zhang J, Duan J, et al. All-inorganic, hole-transporting-layer-free, carbon-based $CsPbIBr_2$ planar perovskite solar cells by a two-step temperature-control annealing process. Mater Sci Semicond Process, 2020, 108, 104870
[67] Huang L, Zhang D, Bu S, et al. Synergistic interface energy band alignment optimization and defect passivation toward efficient and simple-structured perovskite solar Cell. Adv Sci, 2020, 7, 1902656
[68] Jeon N J, Noh J H, Kim Y C, et al. Solvent engineering for high-performance inorganic-organic hybrid perovskite solar cells. Nat Mater, 2014, 13, 897
[69] Ding C, Zhang Y, Liu F, et al. Effect of the conduction band offset on interfacial recombination behavior of the planar perovskite solar cells. Nano Energy, 2018, 53, 17
[70] Deng Q, Li Y, Chen L, et al. The effects of electron and hole transport layer with the electrode work function on perovskite solar cells. Mod Phys Lett B, 2016, 30, 1650341
[71] Yang B, Wang M, Hu X, et al. Highly efficient semitransparent $CsPbIBr_2$ perovskite solar cells via low-temperature processed In_2S_3 as electron-transport-layer. Nano Energy, 2019, 57, 718
[72] Wang Z, Baranwal A K, kamarudin M A, et al. Xanthate-induced sulfur doped all-inorganic perovskite with superior phase stability and enhanced performance. Nano Energy, 2019, 59, 258
[73] Zhu W, Zhang Z, Chai W, et al. Band alignment engineering towards high efficiency carbon-based inorganic planar $CsPbIBr_2$ perovskite solar cells. ChemSusChem, 2019, 12, 2318
[74] Subhani W S, Wang K, Du M, et al. Interface-modification-induced gradient energy band for highly efficient $CsPbIBr_2$ perovskite solar cells. Adv Energy Mater, 2019, 9, 1803785
[75] Correa Baena J P, Steier L, Tress W, et al. Highly efficient planar perovskite solar cells through band alignment engineering. Energy Environ Sci, 2015, 8, 2928
[76] Zhu W, Chai W, Zhang Z, et al. Interfacial TiO_2 atomic layer deposition triggers simultaneous crystallization control and band alignment for efficient $CsPbIBr_2$ perovskite solar Cell. Org Electron, 2019, 74, 103
[77] Wang C, Zhang J, Jiang L, et al. All-inorganic, hole-transporting-layer-free, carbon-based $CsPbIBr_2$ planar solar cells with ZnO as electron-transporting materials. J Alloys Comp, 2020, 817, 152768
[78] Liu C, Li W, Chen J, et al. Ultra-thin MoO_x as cathode buffer layer for the improvement of all-inorganic $CsPbIBr_2$ perovskite solar cells. Nano Energy, 2017, 41, 75
[79] Zhao J, Zhang Y, Zhao X, et al. Band alignment strategy for printable triple mesoscopic perovskite solar cells with enhanced photovoltage. ACS Appl Energy Mater, 2019, 2, 2034
[80] Li Y, Duan J, Yuan H, et al. Lattice modulation of alkali metal cations doped $Cs_{1-x}R_xPbBr_3$ halides for inorganic perovskite solar cells. Solar RRL, 2018, 2, 1800164
[81] Li Z, Zhou F, Wang Q, et al. Approaches for thermodynamically stabilized $CsPbI_3$ solar cells. Nano Energy, 2020, 71, 104634
[82] Zhou Y, Zhou Z, Chen M, et al. Doping and alloying for improved perovskite solar cells. J Mater Chem A, 2016, 4, 17623
[83] Yang Z, Rajagopal A, Jo S B, et al. Stabilized wide bandgap perovskite solar cells by tin substitution. Nano Lett, 2016, 16, 7739
[84] van der Stam W, Geuchies J J, Altantzis T, et al. Highly emissive divalent-ion-doped colloidal $CsPb_{1-x}M_xBr_3$ perovskite nanocrystals through cation exchange. J Am Chem Soc, 2017, 139, 4087
[85] Maughan A E, Ganose A M, Bordelon M M, et al. Defect tolerance to intolerance in the vacancy-ordered double perovskite semiconductors Cs_2SnI_6 and Cs_2TeI_6. J Phys Chem Lett, 2016, 138, 8453
[86] Barker A J, Sadhanala A, Deschler F, et al. Defect-assisted photoinduced halide segregation in mixed-halide perovskite thin films. ACS Energy Lett, 2017, 2, 1416
[87] Tan X, Liu X, Liu Z, et al. Enhancing the optical, morphological and electronic properties of the solution-processed $CsPbIBr_2$ films by Li doping for efficient carbon-based perovskite solar cells. Appl Surf Sci, 2020, 499, 143990
[88] Swarnkar A, Mir W J, Nag A. Can B-site doping or alloying improve thermal- and phase-stability of all-inorganic $CsPbX_3$ (X = Cl, Br, I) perovskites. ACS Energy Lett, 2018, 3, 286
[89] Gangishetty M K, Sanders S N, Congreve D N. Mn^{2+} doping enhances the brightness, efficiency, and stability of bulk perovskite light-emitting diodes. ACS Photonics, 2019, 6, 1111
[90] Zhou F, Li Z, Chen H, et al. Application of perovskite nanocrystals (NCs)/quantum dots (QDs) in solar cells. Nano Energy, 2020, 73, 104757
[91] Liang J, Liu Z, Qiu L, et al. Enhancing optical, electronic, crystalline, and morphological properties of cesium lead halide by mn substitution for high-stability all-inorganic perovskite solar cells with carbon electrodes. Adv Energy Mater, 2018, 8, 1800504
[92] Li N, Zhu Z, Li J, et al. Inorganic $CsPb_{1-x}Sn_xIBr_2$ for efficient wide-bandgap perovskite solar cells. Adv Energy Mater, 2018, 8, 1800525
[93] Subhani W S, Wang K, Du M, et al. Goldschmidt-rule-deviated perovskite $CsPbIBr_2$ by barium substitution for efficient solar cells. Nano Energy, 2019, 61, 165
[94] Zhu W, Chai W, Chen D, et al. Recycling of FTO/TiO_2 substrates: route toward simultaneously high-performance and cost-efficient carbon-based, all-inorganic $CsPbIBr_2$ solar cells. ACS Appl Mater Interfaces, 2020, 12, 4549
[95] Zhu J Y, Lou Y H, Li M, et al. Liquid-chalk painted perovskite films toward low-cost photovoltaic devices. Org Electron, 2019, 75, 105371

[96] Ravi V K, Markad G B, Nag A. Band edge energies and excitonic transition probabilities of colloidal $CsPbX_3$ (X = Cl, Br, I) perovskite nanocrystals. ACS Energy Lett, 2016, 1, 665

[97] Chen W, Zhang J, Xu G, et al. A semitransparent inorganic perovskite film for overcoming ultraviolet light instability of organic solar cells and achieving 14.03% efficiency. Adv Mater, 2018, 30, e1800855

Hushan Zhang received his B.S. degree from Anhui University of Technology in 2015. He is currently a M.S. student at Lanzhou University. His main research focuses on inorganic perovskite based optoelectronic devices.

Zhiwen Jin received the Ph.D. degree from Institute of Chemistry, Chinese Academy of Sciences in 2016, and he joined Lanzhou University in 2018 as a professor with the School of Physical Science and Technology. His research interests include inorganic semiconductor materials, thin-film photoelectric devices and device physics.